

# Incorporating Structured Representations into Pretrained Vision & Language Models Using Scene Graphs

Roei Herzig<sup>\*1,3</sup>, Alon Mendelson<sup>\*1</sup>, Leonid Karlinsky<sup>4</sup>,  
Assaf Arbel<sup>3</sup>, Rogerio Feris<sup>4</sup>, Trevor Darrell<sup>2</sup>, Amir Globerson<sup>1</sup>

<sup>1</sup>Tel-Aviv University, <sup>2</sup>UC Berkeley, <sup>3</sup>IBM Research, <sup>4</sup>MIT-IBM Watson AI Lab

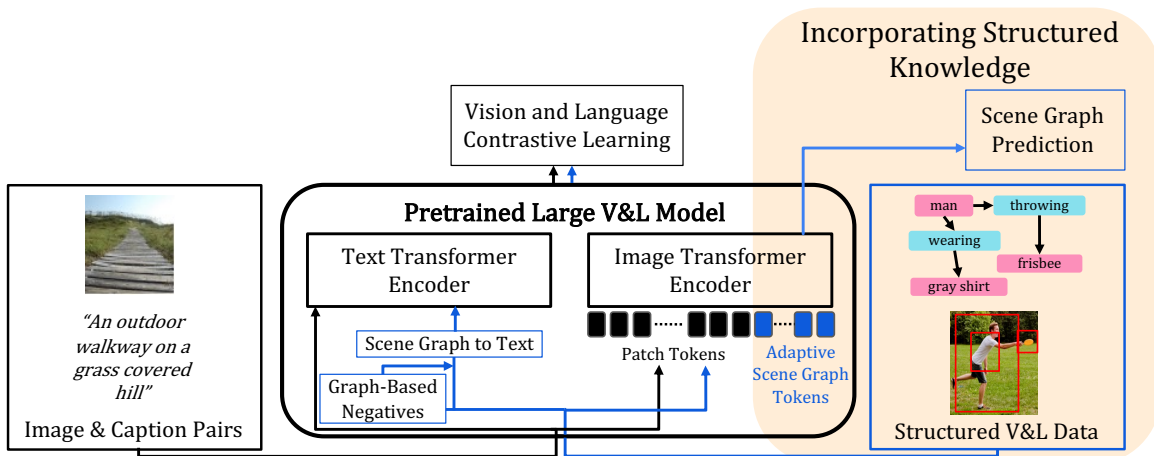


Figure 1: **Scene Graphs Improve Large Vision-Language Models.** Vision and Language (VL) models are typically trained on large-scale image-text pairs (Left). Here we propose to augment training with a small set of scene graphs (SGs) annotations (Right), that is richer and reflects structured visual and textual information. We present a new approach that utilizes image-SG pair data from the Visual Genome [43] dataset, simultaneously trained with the original image-text pairs from LAION [68]. Specifically, we show that it is possible to improve VL models using such data by utilizing a specialized model architecture and a new training paradigm as follows: (i) use the graph to generate fine-grained captions and negative captions that highlight different compositional aspects of the scene. (ii) predict SG information using an open vocabulary approach, by adding special “Adaptive Scene Graph tokens” to the visual encoder that allows better learning of the graph prediction task while still maintaining zero-shot capabilities.

## Abstract

*Vision and Language (VL) models have demonstrated remarkable zero-shot performance in a variety of tasks. However, recent studies have shown that even the best VL models struggle to capture aspects of scene understanding, such as object attributes, relationships, and action states. In contrast, obtaining structured annotations, e.g., scene graphs (SGs) that could improve these models is time-consuming, costly, and tedious, and thus cannot be used on a large scale. Here we ask, can small datasets containing SG anno-*

*tations provide sufficient information for enhancing structured understanding of VL models? We show that it is indeed possible to improve VL models using such data by utilizing a specialized model architecture and a new training paradigm. Our approach captures structure-related information for both the visual and textual encoders by directly supervising both components when learning from SG labels. We use scene graph supervision to generate fine-grained captions based on various graph augmentations highlighting different compositional aspects of the scene, and to predict SG information using an open vocabulary approach by adding special “Adaptive SG tokens” to the visual encoder. Moreover, we design a new adaptation technique tailored*

\*Equal contribution.

specifically to the SG tokens that allows better learning of the graph prediction task while still maintaining zero-shot capabilities. Our model shows strong performance improvements on the Winoground and VL-checklist datasets with only a mild degradation in zero-shot performance.

## 1. Introduction

In recent years, Vision and Language (VL) models (e.g., CLIP [63], BLIP [47]) have shown impressive results across a wide range of tasks, and extraordinary zero-shot capabilities for tasks such as visual question answering, image captioning, and object detection. To achieve these capabilities, these large models are trained on massive datasets containing image-text pairs (e.g., LAION 400M [68]). However, despite the impressive capabilities of these models, recent empirical studies [14, 76, 85] have shown that even the strongest VL models struggle to perform scene understanding, including identifying object attributes and inter-object relations. More broadly, it has been argued that VL models exhibit little compositionality [56].

Understanding the structure of visual scenes is a fundamental problem in machine perception and has been explored extensively in many previous works [10, 25, 49, 81, 83, 87]. In particular, datasets containing scene graph (SG) annotations (e.g., Visual Genome [43]) have been collected and used for training models using structure. While they contribute to scene understanding, these dataset are relatively small and expensive to collect compared to large-scale image-text pair datasets, and thus are not considered in many large VL models.<sup>1</sup> This raises the question: can small datasets containing structured annotations provide sufficient information for finetuning VL models to improve scene understanding? Next, we show that it is indeed possible to improve VL models using such data by utilizing a specialized model architecture and a new training paradigm.

Considering that VL models process both textual and visual representations, these representations must contain structure-related information in order for these models to accurately represent complex scenes. Consequently, our approach incorporates components that directly supervise each of these representations, when learning from SGs paired with images. Our first step is to convert image-SG pairs into image-text pairs, which are natural inputs for VL model training, such that the text accurately describes the structure of the scene graph. A key advantage here is that the resulting captions are dense, and tend to be more exhaustive than in datasets like LAION.

We found that simply introducing these image-caption pairs does not improve performance on Winoground and

VL-Checklist. This is aligned with recent work [16, 84], showing that commonly used contrastive learning approaches allow the model to concentrate mainly on object labels disregarding other important aspects, such as relations and attributes. To further introduce structure, we observe that SGs can be used naturally to generate hard-negatives. For example, if an SG contains an edge “dog-chasing-cat”, then we can reverse that edge “cat-chasing-dog” and generate a corresponding negative caption. A contrastive loss between the negative and the original captions can be used to force the model to focus on finer details.

We next turn to introduce structure into the visual representation. Intuitively, we would like the visual encoder to capture structure-related information. We argue that this can be achieved via predicting scene graph information from the visual encoder by adding tokens that are designed to capture objects and relations, inspired by prompt learning approaches [35, 24, 92, 90]. We refer to these as “adaptive scene graph tokens” and train them to predict scene graph information directly using an open vocabulary approach, which predicts objects and relations described by text inputs rather than relying on a fixed vocabulary.

Finally, integrating complex structured knowledge into large VL models using standard finetuning techniques may result in catastrophic forgetting, as shown recently [13, 16]. To alleviate this issue, we design a new adaptation technique tailored specifically to the prompting approach. In particular, we modify the transformer layers by adding parameters that are specific to the SG tokens, so that the SG component has a reduced effect on VL parameters. We name our proposed approach SGVL (*Scene Graphs for Vision-Language Models*). See Figure 1 for an overview.

To summarize, our main contributions are as follows: (i) we propose to exploit a small set of SG annotations to incorporate structured representations into pretrained large VL models. (ii) we propose a new approach that captures structure-related information for both encoders by directly supervising the visual and textual components when learning from SG labels. (iii) we further design a new adaptation technique tailored specifically to the SG tokens that allows better learning of the graph prediction task while still maintaining zero-shot capabilities; (iv) our method shows improved performance upon CLIP [63] and BLIP [47] on the Winoground [76] and VL-CheckList [89] datasets with only a mild degradation in zero-shot performance, highlighting the effectiveness of the proposed approach.

## 2. Related Work

**Vision and Language (VL) Models.** In recent years, VL models [11, 18, 22, 34, 47, 50, 63, 69] have emerged as powerful models for a wide range of tasks, demonstrating extraordinary zero-shot capabilities. These models are trained with image-text pairs in order to align the

<sup>1</sup>Visual Genome contains approximately 100K image-SG pairs, which is  $\times 1000$  smaller than the large-scale VL models pretraining datasets.

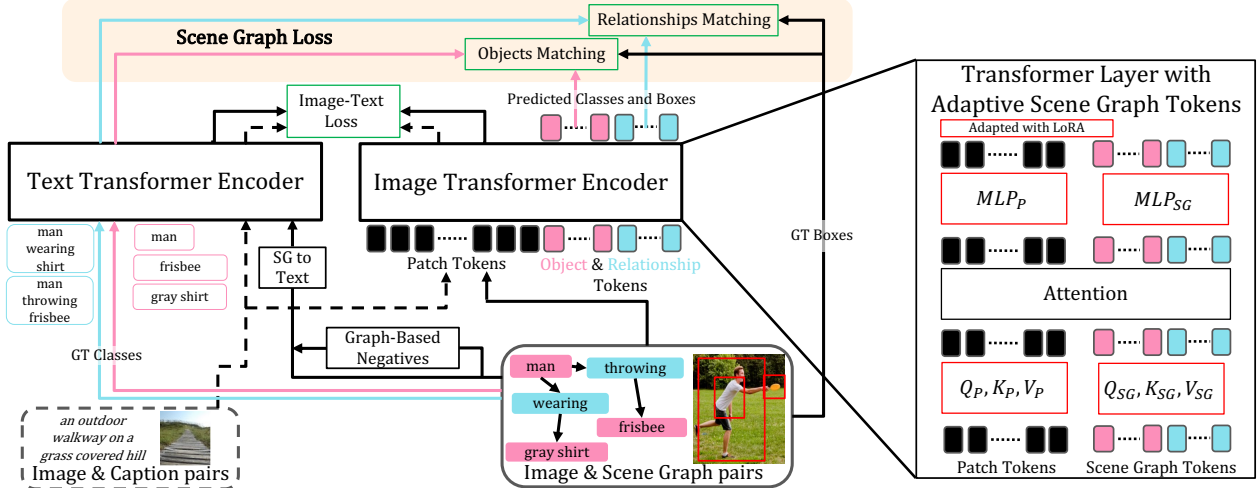


Figure 2: **Our Scene Graphs for Vision-Language Models (SGVL) Approach.** Our approach trains simultaneously on image-SG pairs (black solid arrows) and “standard” image-text pairs (black dotted arrows). Our key aspect is to capture structure-related information in both visual and textual components, when learning from scene graph labels. For the textual side, we generate captions and negative captions using the graph (Graph-Based Negatives and SG to text modules). For the visual side, we predict SG information (classes and boxes) by adding tokens that are intended to capture objects (pink tokens & arrows) and relationships (cyan tokens & arrows), and these predictions are supervised with ground truth labels using bipartite matching. The object and relationship class labels are matched in embedding space between SG token representations and textual embeddings of ground truth classes. Finally, our new adaptation technique, shown in the figure on the right, is tailored specifically to the SG tokens and allows better learning of the graph prediction and VL tasks.

two modalities in a joint embedding space. More recently, popular vision-language methods, such as CLIP [63], CyCLIP [22], BLIP [47], ALIGN [34], PyramidCLIP [18], and others, have proposed bridging the two modalities by learning two encoders simultaneously. The advantage of large-scale pretraining is exploited by these models through the use of large neural networks and large datasets. However, recent empirical studies (e.g., VL-CheckList [89], Winoground [76], and the recent ARO [84] benchmark) have shown that these models do not perform well on tasks that require understanding of the structure of the image, including identifying relations between objects and mapping between objects and attributes. Moreover, recent research [16] has shown that these models tend to learn a representation of a “bag of objects”, leading them to be less structure-aware. Here we show that even training with a small number of structured annotations can contribute to gaining this structured knowledge for large VL models.

**Parameter Efficient Finetuning Techniques.** Recently, several approaches have been proposed for efficient large model fine-tuning, such as prompt learning [92, 90], using adapters [29, 64, 52], finetuning part of the model [8, 73], etc. Recently, prompt tuning [45] has been proposed as an approach to treating prompts as task-specific continuous vectors and directly optimizing them via gradients, particularly in VL models [2, 19, 24, 35, 38, 63, 67, 91]. A key principle behind these works is to gain efficiency over full fine-tuning by achieving comparable performance while storing fewer parameters. Other popular approaches

have used adapters [29, 64, 52] to enhance efficiency by fine-tuning models with fewer parameters. Adapters have been introduced as powerful modules added to frozen layers, in which only the adapter parameters are updated. They have been widely used to avoid catastrophic forgetting in multiple topics, such as NLP [30, 4], VL [72, 57], continual learning [70], video understanding [52], and more. Unlike these works, here, we add special tokens that are designed to capture objects and relations, supervised by SG annotations rather than the main contrastive loss. Since SG prediction is challenging and may result in large parameter changes in training, we modify the transformer layers by adding parameters specific to these tokens to minimize the impact on VL parameters. This allows us to maximize the potential of the structured task without losing zero-shot performance.

**Learning Structured Representations.** Structured representations have been shown beneficial in many computer vision applications: video understanding [1, 3, 20, 21, 26, 27, 33, 55, 58, 59, 71, 75, 78, 79, 88], relational reasoning [6, 7, 28, 42, 32, 62, 82, 86], vision and language [12, 48, 50, 74], human-object interactions [17, 39, 80], and even image & video generation [5, 25, 36]. In recent years, SGs [37, 81] have been extensively used to provide semantic representations that have been applied in a wide range of applications. However, in this work, we demonstrated that even a small amount of scene graph annotations compared to a large-scale image-text pairs datasets can be used to incorporate structured knowledge into large VL models.

### 3. Scene Graphs for Vision-Language Models

We begin by describing the standard VL transformer architecture, the scene graph annotations, and the problem setup (Section 3.1). We then introduce our structural considerations for both the language (Section 3.2) and vision (Section 3.3) encoders, and the training losses (Section 3.4). Our method is illustrated in Figure 2.

#### 3.1. Preliminaries

VL models are typically trained with pairs of images and texts:  $X_i = (I_i, T_i)$ . Each of these modalities is processed by a separate transformer encoder, and the objective of training is to map the embeddings of images and their corresponding texts to nearby positions, usually via a contrastive loss. Next, we briefly describe the encoders.

**Language Transformer Encoder  $E_T$ .** The text encoder is a transformer [77] as described in CLIP [63] and BLIP [47], where a CLS token is appended to the beginning of the text, and the final CLS embedding is used as the text embedding.

**Vision Transformer Encoder  $E_I$ .** A typical vision transformer model [15] (ViT) takes an image  $I \in \mathbb{R}^{3 \times H \times W}$  as input, extracts  $N$  non-overlapping patches, and projects them into a lower-dimension  $d$ . We refer to these patches as “patch tokens”, and denote them  $PT_i$ . Then, spatial position embeddings  $PE \in \mathbb{R}^{N \times d}$  are added to provide spatial location information, resulting in a new embedding:  $z_i = PT_i + PE_i$ . This forms the sequence of input tokens to the vision transformer encoder:

$$z = [z_{CLS}, z_1, z_2, \dots, z_N] \quad (1)$$

where  $z_{CLS}$  is a learnable token. The input  $z$  is fed into a standard transformer, and the final representation of the CLS token is the image embedding.

**Scene Graphs (SGs).** As mentioned above, our motivation is to improve VL models by leveraging structured annotations from a scene graph dataset. The nodes of the scene graph represent objects and the edges correspond to relationships. Formally, an SG is a tuple  $G = (V, E)$  defined as follows: (i) *Nodes  $V$*  - A set  $V$  of  $n$  objects. Every object in the scene graph contains a class label, a bounding box, and attributes. (ii) *Edges  $E$*  - A set  $E$  of  $m$  edges. These relationships are triplets  $(i, e, j)$  where  $i$  and  $j$  are object nodes, and  $e$  is the category of the relation between objects  $i$  and  $j$ .

**Problem Setup.** As mentioned above, we assume access to image-SG pairs  $(I_G, G)$  from Visual Genome to improve structured understanding while training simultaneously with the original image-text pairs from LAION. Since the scene graphs can be quite large, we simplify them and generate sub-graphs, along with corresponding image crops. For more details, see Section A.1.

Next, we describe the textual and visual structured components that capture structure in both modalities.

### 3.2. Structural Language Component

We begin by discussing how an SG is transformed into text, and then explain how to manipulate the SG with our Graph-Based Negatives to further capture structure in the model. For a visualization, see Figure 4 in supplementary.

**Scene Graph to Text.** Given an Image  $I$  and a corresponding scene graph  $G = (V, E)$  from the training dataset, we use the graph  $G$  to generate a textual caption for the image. We start by iterating over the connected components of the graph one by one and generate a textual caption for each component by concatenating the class labels from the graph edges over a Hamiltonian path. We prepend a corresponding attribute before the object class label if such exists. Last, we generate a single caption by concatenating the captions of the connected components separated by a dot. For a visualization, see Figure 4 in supplementary.

**Graph-Based Negatives (GN).** We have found that using the scene graph data solely as image-text pairs with the contrastive loss is not enough to force the model to develop structural understanding. As shown in recent work [16, 84], the commonly used contrastive learning allows the model to concentrate mainly on object labels disregarding other important aspects, such as relations and attributes. In order to provide more focus on such aspects, we exploit the SG structure and propose a set of predefined graph-based rules (See Section A.2) that modify SGs and make them semantically inconsistent with the image. Next, these SGs are transformed into negative textual captions, which are used with a specified loss to motivate the model to focus on structural aspects. For a visualization, see Figure 4 in supplementary.

### 3.3. Structural Visual Component

**Scene Graphs Tokens.** As mentioned earlier, a natural way to capture structure-related information in the visual encoder is to use it to predict scene graphs. Towards this end, we add a set of “SG tokens” that are learned queries and are designed to predict objects and relationship from the graph. The SG tokens consist of two groups. The first are “object tokens” meant to represent objects, their locations and their attributes. The second are “relationship tokens” meant to represent SG edges that describe relationships.

Formally, we define a fixed set of  $\tilde{n}$  learned object queries and denote them by  $p_1^o, p_2^o, \dots, p_{\tilde{n}}^o \in \mathbb{R}^{1 \times d}$ . Similarly, we define a fixed set of  $\tilde{m}$  relationships queries and denote them by  $p_1^r, p_2^r, \dots, p_{\tilde{m}}^r \in \mathbb{R}^{1 \times d}$ . We refer to these queries as the learned SG tokens. We note that  $\tilde{n} > n_{max}$ ,  $\tilde{m} > m_{max}$ , where  $n_{max}/m_{max}$  is the maximal number of objects/relationships. This implies that some queries predict the categories “no object” and “no relationship”.

The scene graph tokens are concatenated with the standard CLS and patch tokens to obtain the following set of

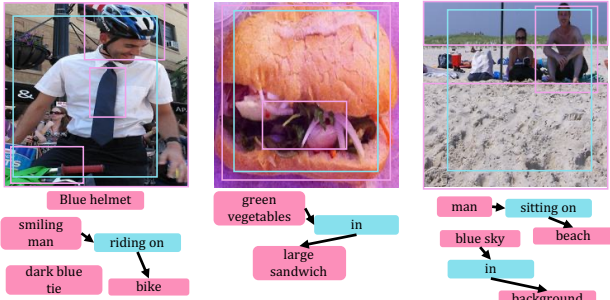


Figure 3: “Scene Graph Tokens” Visualization. The predictions of object tokens (pink) and relationship tokens (cyan) are shown for images not in the Visual Genome training data.

inputs to the transformer:

$$z = [z_{CLS}, z_1, z_2, \dots, z_N, p_1^o, p_2^o, \dots, p_n^o, p_1^r, p_2^r, \dots, p_n^r] \quad (2)$$

Next, the transformer processes the input  $z$ , resulting in a new representation for each token (i.e., the CLS token, the SG tokens, and the patch tokens). Given an input image  $I$  that induces an input  $z$ , we denote  $F_O^j(I)$ ,  $F_R^k(I)$  the representations of the  $j^{\text{th}}$  object token and  $k^{\text{th}}$  relationship token. We use these representations to predict object and relationship labels and localization, by passing them through two feed-forward networks (see Equation 8). These predictions are supervised with ground-truth SGs annotations through a matching process. Figure 3 visualizes the SG tokens learned by our model. More details are in Section 3.4.

**Adaptive tokens.** Our training approach is to fine-tune an existing VL model on the SG data, with the added SG tokens. The finetuning of machine learning models may result in catastrophic forgetting, and therefore the model may lose its VL skills, including zero-shot capabilities. This is of special concern in our setup, as the task of scene graph prediction is challenging and deviates significantly from the initial training scheme of the model, potentially resulting in large changes in the parameters. To alleviate this issue, we design a new adaptation technique tailored specifically to the prompting approach. We propose to add parameters that are specific to the SG tokens, so that the SG component has a reduced effect on VL parameters. Recall that transformer layers have matrices for mapping to queries, keys and values. We denote these matrices for the pretrained VL model by  $Q_P, K_P, V_P$ . The SG tokens we add could have used the same matrices. However, we have found that the SG prediction task does not converge well using this setup, and thus we introduce a separate set of matrices  $Q_{SG}, K_{SG}, V_{SG}$  that is used with the SG tokens. Importantly, the attention is performed over *all* tokens (patch and SG). Similarly, for the MLP component in the transformer layer, we also have a different version for the patch tokens (denoted by  $MLP_P$ ) and the SG tokens (denoted by  $MLP_{SG}$ ).

Finally, we also use Low Rank Adapters (LoRA [30]), which restrict the parameter updates to low-rank matrices, and have been shown to be effective in fine-tuning of transformers. Specifically, for each trainable matrix  $W \in \mathbb{R}^{u \times v}$  (e.g.,  $W = Q_P$  or  $W = Q_{SG}$ ) we let  $W_0$  denote its pre-trained weights, and parameterize the learned matrix as:

$$W = W_0 + AB \quad (3)$$

where  $A \in u \times r$  and  $B \in r \times v$  are  $r$ -rank matrices and  $r$  is a hyperparameter.<sup>2</sup> We note that we use two distinct  $r$ :  $r_P$  and  $r_{SG}$  for weights associated with the patch tokens and SG tokens (as described above), respectively. This allows the use of a higher rank for the SG parameters in order to perform better at the SG prediction. During training,  $W_0$  is kept frozen, while  $A, B$  are learned. Overall, our additional trainable parameters are only 7.5% of the model.

**Open Vocabulary Scene Graph Prediction.** The annotated SGs contain category information (for objects, relationships and attributes). Our SG tokens are meant to predict these categories. Naive implementation of this idea would require a prediction head with an output for each category. However, the VG dataset contains approximately 70K object categories and 40K relationship categories, and thus poses a significant challenge in terms of handling the imbalanced, limited, and sparse nature of the data. One possible solution [81] introduced a split containing only 100 object labels and 50 relation labels, which further restricted the already small dataset. Rather than restricting our data, we use an open vocabulary approach, namely, we utilize the text encoder to embed the categories from the SG components. Next, we use these embeddings in training to supervise the SG tokens. For example, if node  $i$  has category “dog” and attribute “black”, we train some object token to predict the embedding of the phrase “black dog”. This also applies to the prediction of relationship tokens, which might be the embedding of the relationship “dog chasing cat”. More details are in Scene Graph Loss in Section 3.4.

### 3.4. Training and Losses

As previously mentioned, we use CLIP [63] and BLIP [47] that both include a transformer image encoder  $E_I$  and transformer text encoder  $E_T$ . The similarity between an image  $I$  and a text  $T$  is calculated as follows:

$$\text{sim}(I, T) := \cos(E_I(I), E_T(T)) \quad (4)$$

where  $\cos$  is the cosine similarity.

As previously described (Section 3.2), during training we have a set of image-text pairs  $(I, T)$  and a set of image-SG pairs  $(I_G, G)$ . We use the image-SG pairs to generate a set of images with positive textual captions  $(I_G, T^p)$  and

<sup>2</sup>For the SG-token parameters, we set  $W_0$  to the value of the corresponding parameters of the patch tokens.

Model	Winoground			VL-Checklist			21 Zero-Shot Tasks Average
	Text	All Dataset Image	group	All Datasets Average Attribute	Object	Relation	
Random Chance	25.0	25.0	16.7	50.0	50.0	50.0	-
LXMERT [74]	27.5	8.7	6.0	71.4	82.4	69.4	-
UNITER <sub>base</sub> [12]	32.2	13.2	10.0	68.0	81.9	75.3	-
ViLT (ViT-B/32) [40]	34.7	14.0	9.2	72.2	86.3	75.6	-
CLIP (ViT-B/32) [63]	30.7	10.5	8.0	65.5	80.6	78.0	56.4
BLIP (ViT-B/16) [47]	39.0	19.2	15.0	75.2	82.2	81.5	49.0
CLIP-SGVL (ours)	32.0 (+1.3)	14.0 (+3.5)	9.8 (+1.8)	71.2 (+5.7)	82.6 (+2.0)	79.0 (+1.0)	53.3 (-3.1)
BLIP-SGVL (ours)	39.0	30.5 (+11.3)	21.5 (+6.5)	78.2 (+3.0)	85.2 (+3.0)	80.4 (-1.1)	48.0 (-1.0)

Table 1: **Winoground and VL-Checklist Summary Results.** The **gains** and **losses** are in color.

negative textual captions ( $I_G, T^n$ ). We use these as inputs to our model (3), while optimizing the following losses:

**Image-Text Loss.** Our image-text loss is comprised of two terms, *contrastive loss* and *graph negatives loss*.

*Contrastive Loss:* The standard approach to train VL models is via contrastive loss on image-text pairs, as in [63]. We do this here with the standard pairs ( $I, T$ ) and those generated from the scene graphs ( $I_G, T^p$ ). Thus, the loss is:

$$\mathcal{L}_{cont} := \text{contrastive}(E_I(\tilde{I}), E_T(\tilde{T})) \quad (5)$$

where  $\tilde{I} = I \cup I_G$  and  $\tilde{T} = T \cup T^p$ .

*Graph-Based Negative Loss:* For each image with an SG, we have a text  $T^p$  that faithfully describes it, and a negative text  $T^n$  that does not describe it. We thus use a loss that drives  $T^p$  to be more similar to  $I_G$  than  $T^n$  (e.g., see [16]):

$$\mathcal{L}_{GN} := \sum_{I_G, T^p, T^n} -\log \left( \frac{e^{\text{sim}(I_G, T^p)}}{e^{\text{sim}(I_G, T^p)} + e^{\text{sim}(I_G, T^n)}} \right) \quad (6)$$

Finally, the image-text loss is a weighted sum of the contrastive loss and the graph negatives loss:

$$\mathcal{L}_{IT} := \mathcal{L}_{cont} + \lambda_{GN} \mathcal{L}_{GN} \quad (7)$$

where  $\lambda_{GN}$  is a hyperparameter. As in the BLIP [47] paper, we use the image-text matching module to apply a loss to all image-text pairs. We also add an additional term to the Graph-based Negative loss that uses this module. See Section A.4 in supplementary.

**Scene Graph Loss.** As mentioned in Section 3.3, we incorporate SG tokens into the model, which are used to predict the SG that corresponds to the image. We next explain this process. The graph  $G$  contains several annotations: the set of object categories  $O = \{o_i\}_{i=1}^n$ , the set of bounding boxes  $B^O = \{b_i^o\}_{i=1}^n$ , and set of relationship categories  $R = \{r_i\}_{i=1}^m$ . We also augment the relationships with a set of bounding boxes, that are constructed as the union of the boxes of the corresponding objects, and denote these by  $B^R = \{b_i^r\}_{i=1}^m$ .

As mentioned, we do not aim to predict the object and relationship categories directly, but rather use the embeddings from the VL model. Thus, we extract the embeddings of these labels with the text encoder  $E_T$  to get class embeddings:  $\hat{O} = E_T(O) \in \mathbb{R}^{(n+1) \times d}$ , and  $\hat{R} = E_T(R) \in \mathbb{R}^{(m+1) \times d}$ . We note that  $(n+1)$  and  $(m+1)$  classes are due to “no object” and “no relationship” categories (denoted as  $\emptyset$ ), which are represented with learned embeddings.

Thus far we described the elements of the SG that we aim to predict from the SG tokens. We next describe the prediction process, and the corresponding losses. The image encoder outputs a set of  $\tilde{n}$  object queries and  $\tilde{m}$  relationship queries. We apply two feed-forward networks,  $\text{FFN}_{bb}$  and  $\text{FFN}_e$ , on top of these queries to predict bounding boxes and label embeddings respectively. Specifically, given the  $j^{\text{th}}$  object token and  $k^{\text{th}}$  relationship token, we predict

$$\hat{b}_j = \text{FFN}_{bb}(F_O^j(I)), \hat{e}_j = \text{FFN}_e(F_O^j(I)) \quad (8)$$

$$\hat{b}_k = \text{FFN}_{bb}(F_R^k(I)), \hat{e}_k = \text{FFN}_e(F_R^k(I)) \quad (9)$$

where  $\hat{b}_j, \hat{b}_k \in \mathbb{R}^{1 \times 4}$  are bounding box predictions and  $\hat{e}_j, \hat{e}_k \in \mathbb{R}^{1 \times d}$  are class embeddings predictions. Next, we use the class embeddings matrices to predict probabilities over  $n+1$  and  $m+1$  classes:

$$\hat{q}_j^o = \text{SoftMax}(\hat{e}_j \hat{O}^T), \hat{q}_k^r = \text{SoftMax}(\hat{e}_k \hat{R}^T) \quad (10)$$

where  $\hat{q}_j^o \in \mathbb{R}^{1 \times n+1}$  and  $\hat{q}_k^r \in \mathbb{R}^{1 \times m+1}$ . Next, we need to match the predictions of the SG tokens with the ground-truth SG, in order to determine which SG tokens correspond to which GT objects and relationships. We follow the matching approach as in DETR [9], except that in our case, objects and relationships are matched separately. For example, for the objects, this matching process checks the compatibility between GT and permuted objects in terms of object category (i.e., the probability assigned by the query to the GT object  $o_i$ ) and in terms of bounding boxes (i.e., how well the predicted box matches the GT one). With the

Model	NoTag			Visually Difficult			Complex Reasoning		
	Text	Image	group	Text	Image	Group	Text	Image	Group
CLIP [63]	30.4	11.1	8.2	15.8	0.0	0.0	24.4	7.7	3.8
BLIP [47]	44.8	23.8	19.0	29.0	10.5	10.5	24.4	7.7	2.6
CLIP-SGVL (ours)	33.2 (+2.8)	14.0 (+2.9)	8.7 (+0.5)	18.4 (+2.6)	5.3 (+5.3)	5.3 (+5.3)	24.4	16.7 (+9.0)	12.8 (+9.0)
BLIP-SGVL (ours)	44.2 (-0.6)	37.8 (+14.0)	26.2 (+7.2)	23.7 (-5.3)	21.0 (+10.5)	15.8 (+5.3)	28.2 (+3.8)	10.2 (+2.5)	6.4 (+3.8)

Table 2: **Winoground Results** on the NoTag, Visually Difficult and Complex Reasoning splits.

model	Attribute					Object		Relation
	Action	Color	Material	Size	State	Location	Size	Action
CLIP [63]	68.1	70.2	73.1	52.9	63.3	81.0	80.1	78.0
BLIP [47]	79.5	83.2	84.7	59.8	68.8	83.0	81.3	81.5
CLIP-SGVL (ours)	76.6 (+8.5)	78.0 (+7.8)	80.6 (+7.5)	59.7 (+6.8)	61.2 (-2.1)	83.2 (+2.2)	81.9 (+1.8)	79.0 (+1.0)
BLIP-SGVL (ours)	77.6 (-1.9)	87.0 (+3.8)	86.6 (+1.9)	68.3 (+8.5)	71.3 (+2.5)	86.5 (+3.5)	83.9 (+2.6)	80.4 (-1.1)

Table 3: **VL-Checklist Result** on the Attribute, Object, and Relation tests, excluding the Visual Genome dataset.

optimal matching  $\hat{\sigma}$  we calculate the following Objects loss:

$$\mathcal{L}_{Obj} = \sum_{i=1}^{\tilde{n}} \left[ -\log \hat{q}_{\hat{\sigma}(i)}^o(o_i) + \mathbb{1}_{\{o_i \neq \emptyset\}} \mathcal{L}_{Box}(b_i^o, \hat{b}_{\hat{\sigma}(i)}) \right] \quad (11)$$

where  $\mathcal{L}_{Box}$  is a weighted combination of  $\mathcal{L}_{giou}$  [65] and  $\mathcal{L}_1$  losses. The relationship loss  $\mathcal{L}_{Rel}$  is calculated in a similar manner, and the total loss is the sum of these losses. Finally, our method can be applied on top of a variety of VL models. For our experiments, we use the CLIP [63] and BLIP [47] models. The complete matching and losses details are in Section A.3.

## 4. Experiments and Results

### 4.1. Datasets

For training, we use the LAION dataset as “standard” image-text pairs, along with SG data from Visual Genome (VG). For evaluation we use the VL-Checklist [89] and Winoground datasets, as well as zero-shot classification tasks. **(1) LAION 400M** [68] is a large-scale image-text pair dataset that was automatically curated from the Internet and has been filtered using the pretrained CLIP model. LAION 400M has been used to reproduce CLIP and it achieves similar performance to the original model [63]. **(2) Visual Genome** [43] (VG) is annotated with 108,077 images and scene graphs. On average, images have 12 entities and 7 relations per image. For the datasets that are used for testing: **(1) VL-Checklist** [89] is a new study that combines the following datasets: Visual Genome [43], SWiG [61], VAW [60], and HAKE [51]. For each image, two captions are given, a positive and a negative. The positive caption is coherent with the visual structure of the image, and the negative caption is constructed by modifying one word in the positive caption that corresponds to a structural visual aspect (e.g., attribute). We report results on a com-

bined VL-Checklist datasets excluding Visual Genome<sup>3</sup>. For more details see Section D.1 **(2) Winoground** [76] is a dataset that probes compositionality in VL models. The dataset contains 400 samples, each composed of two image-text pairs. The pairs have overlapping lexical content but are differentiated by a swapping of an object, a relation, or both. Each sample tests the performance on two text-retrieval tasks (text score), and two image retrieval tasks (image score). The combined performance is represented by the group score. A recent study [14] has shown that solving Winoground requires not just compositionality but also other abilities such as commonsense reasoning. The study proposed a new split to Winoground differentiating the samples by the source of their hardness. Along our work we use this suggested split, For more info, Section D.2.

**Zero-Shot Classification.** Our method was evaluated using 21 classification datasets following the Zero-Shot classification protocol described in ELEVATER [46]. The evaluation includes common classification datasets such as ImageNet [66], CIFAR100 [44], EuroSat [23], and others. We report the average results over the 21 tasks in Table 1.

### 4.2. Implementation Details

We have implemented SGVL using Pytorch, and the code will be released upon acceptance and is included in the supplementary. Our code and training procedures are based on CLIP and BLIP. For CLIP [63], we use the ML-Foundation Open-CLIP repository [31], and for BLIP [47] we use the official implementation<sup>4</sup>. We use the ViT/B-32 model architecture for CLIP and ViT/B-16 for BLIP. The models are initialized with original weights released by the respective authors. For more info, please refer to Section D.

<sup>3</sup>For example, we do not include spatial relations in our evaluation.

<sup>4</sup><https://github.com/salesforce/BLIP>

(a) Scene Graph Information				(b) Visual Encoder Components				(c) Image-SG Comprehensiveness			
Model	Text	Image	Group	Model	Group $\uparrow$	ZS $\uparrow$	IoU $\downarrow$	Model	Text	Image	Group
BLIP	39.0	19.2	15.0	BLIP	15.0	49.0	-	30% of Graph	33.2	26.5	18.0
BLIP + Graph Text	41.7	17	15.2	BLIP MT	17.5	47.0	0.9	70% of Graph	38.7	27.7	20.2
BLIP + Graph Text + GN	40.5	25.5	18.2	BLIP + SG Tokens	19.2	47.5	0.6	w/o Relations	40.5	20.5	15.8
BLIP + Graph Text + GN + SG Tokens	39.0	30.5	21.5	BLIP + Adaptive SG Tokens	21.5	48.0	0.3	Entire Graph	39.0	30.5	21.5

Table 4: **Ablations on the Winoground Dataset.** We report Text, Image, and Group scores. We show (a) The contribution of scene graph information. (b) Method components, and (c) Image-SG comprehensiveness. More ablations are in Section B in supplementary.

### 4.3. Baselines

We compare SGVL to two models reported in previous work. The first is CLIP [63], the OpenAI pretrained model, which was trained on 400M image-text pairs and achieves high zero-shot results. Second, we consider the recent BLIP [47] model, which shows improved results on VL understanding tasks. To ensure a fair comparison, all methods use the same network architecture and initialization from the respective pretrained models. We provide additional results in Section B in the supplementary.

The evaluation of Winoground and VL-Checklist requires matching images and texts. We follow the standard protocols for CLIP and BLIP. Namely, for CLIP, we compute the cosine similarity between the image and the text CLS embeddings. For BLIP, we use the ITM module that predicts a positive-negative score for an image-text pair.

### 4.4. Results

We evaluate our method on Winoground and VL-Checklist, and the results are shown in Table 1. On Winoground, CLIP-SGVL improves the image, text, and group scores, while BLIP-SGVL improves the image and group scores significantly, and the text score remains comparable. We note that our BLIP-SGVL is the first to report above chance level results on all three Winoground score splits (See “Random Chance”). On VL-Checklist, CLIP-SGVL improves all tasks, and BLIP-SGVL achieves gains on the “Attribute” and “Object” tests, while the results for the “Relation” test slightly degrade. We note that these improvements come at the price of some degradation in Zero-Shot performance compared to CLIP and BLIP models.

Table 2 shows our performance on fine-grained Winoground splits. We report the NoTag, Visually Difficult and Complex Reasoning splits, as introduced [14]. The first split measures compositional understanding, while the second tests the detection quality of visual elements. To resolve the last category, common sense reasoning or world knowledge is required. It can be seen that our approach incorporates well structure in order to enhance compositionality, detection quality, and common sense reasoning.

Last, Table 3 shows improvements on VL-Checklist. Specifically in the “Attribute” and “Object” categories we show consistent improvements for CLIP-SGVL and BLIP-SGVL. For the “relation” category, we assume that our graph-based negatives do not focus as much on action re-

lations as they do on spatial relations (which is more representative of the scene graphs from VG).

### 4.5. Ablations

We perform an ablation study on the Winoground [76] dataset with our SGVL approach using the BLIP model (See Table 4). For more ablations, see Section B.2 in supp.

**Scene Graph Information.** To validate the best way of utilizing the SG information, Table 4a illustrates how the visual and textual components contribute to the approach. By adding only the textual description generated from the SGs (BLIP + Graph Text in the table), we obtain the following Text/Image/Group scores over the BLIP baseline: +2.7/-2.2/-0.2. The results compared to the baseline improves to +1.5/+6.3/+3.2 when the graph-based negatives (GN) are included, demonstrating the effectiveness of the generated negatives. Moreover, when the SG tokens are added, the image/group scores significantly improved by +11.3/6.5, whereas the text score remains comparable. This highlights that supervising both visual and textual components when learning from SG labels is beneficial.

**Visual Encoder Components.** In this ablation, we justify our design choices within the visual encoder, as we use the same generated captions and negatives for all variants. We report performance in Table 4b on three different tasks: Winoground (group score), Zero-shot classification (ZS), and SG prediction (IoU metric).

To measure the contribution of the SG tokens, we propose an alternative variant, *BLIP MT* (BLIP Multi-Task), which does not include SG tokens and predicts the graph using the CLS token. It can be seen that the *BLIP+SG Tokens* outperforms the *BLIP MT*, demonstrating the benefits of the SG tokens. Last, our “adaptive SG tokens” outperforms all other models, demonstrating that our proposed adaptation technique tailored to the SG tokens indeed allows better learning of the SG prediction task and Winoground while still maintaining zero-shot capabilities.

**Image-SG Comprehensiveness.** To examine the significance of SG comprehensiveness with respect to the image, we train our model with partial graphs. Specifically, we train two variants where objects and relations from the graphs are randomly removed (30% and 70%) and a third variant in which all relations are removed. As can be seen in Table 4c, our results show that our model performs better when the graphs are denser, richer, and describe the image more accurately, highlighting the motivation to utilize SGs.



## 5. Discussion and Limitations

Structured understanding of complex scenes is a key element of human visual perception, but its modeling still remains a challenge. In this work, we propose a new approach for incorporating structured information into pretrained VL models from a small set of SGs annotations to improve performance of scene understanding. We demonstrate improved performance on Winoground and VL-CheckList with only a mild degradation in zero-shot performance. Although our work exploits SG annotations, it is important to note that these annotations are limited in availability and are expensive. Therefore, we leave for future work the challenge of using our approach in an unsupervised manner.

### Acknowledgements

This project has received funding from the European Research Council (ERC) under the European Unions Horizon 2020 research and innovation programme (grant ERC HOLI 819080). Prof. Darrell’s group was supported in part by DoD, including PTG and/or LwLL programs, as well as BAIR’s industrial alliance programs. IBM research was supported by DARPA under Contract No. FA8750-19-C-1001.

### References

- [1] Anurag Arnab, Chen Sun, and Cordelia Schmid. Unified graph structured models for video understanding. In *ICCV*, 2021. 3
- [2] Akari Asai, Mohammadreza Salehi, Matthew E. Peters, and Hannaneh Hajishirzi. Attentional mixtures of soft prompt tuning for parameter-efficient multi-task knowledge sharing. *ArXiv*, abs/2205.11961, 2022. 3
- [3] Elad Ben Avraham, Roei Herzig, Karttikeya Mangalam, Amir Bar, Anna Rohrbach, Leonid Karlinsky, Trevor Darrell, and Amir Globerson. Bringing image scene structure to video via frame-clip consistency of object tokens. In *Thirty-Sixth Conference on Neural Information Processing Systems*, 2022. 3
- [4] Ankur Bapna and Orhan Firat. Simple, scalable adaptation for neural machine translation. In *Proceedings of the 2019 Conference on Empirical Methods in Natural Language Processing and the 9th International Joint Conference on Natural Language Processing (EMNLP-IJCNLP)*, Nov. 2019. 3
- [5] Amir Bar, Roei Herzig, Xiaolong Wang, Anna Rohrbach, Gal Chechik, Trevor Darrell, and A. Globerson. Compositional video synthesis with action graphs. In *ICML*, 2021. 3
- [6] Fabien Baradel, Natalia Neverova, Christian Wolf, Julien Mille, and Greg Mori. Object level visual reasoning in videos. In *ECCV*, pages 105–121, 2018. 3
- [7] Peter W Battaglia, Jessica B Hamrick, Victor Bapst, Alvaro Sanchez-Gonzalez, Vinicius Zambaldi, Mateusz Malinowski, Andrea Tacchetti, David Raposo, Adam Santoro, Ryan Faulkner, et al. Relational inductive biases, deep learning, and graph networks. *arXiv preprint arXiv:1806.01261*, 2018. 3
- [8] Elad Ben-Zaken, Shauli Ravfogel, and Yoav Goldberg. Bit-fit: Simple parameter-efficient fine-tuning for transformer-based masked language-models. *ArXiv*, abs/2106.10199, 2021. 3
- [9] Nicolas Carion, Francisco Massa, Gabriel Synnaeve, Nicolas Usunier, Alexander Kirillov, and Sergey Zagoruyko. End-to-end object detection with transformers. In Andrea Vedaldi, Horst Bischof, Thomas Brox, and Jan-Michael Frahm, editors, *Computer Vision – ECCV 2020*, pages 213–229, 2020. 6, 1
- [10] Shizhe Chen, Pierre-Louis Guhur, Makarand Tapaswi, Cordelia Schmid, and Ivan Laptev. Language conditioned spatial relation reasoning for 3d object grounding. *ArXiv*, abs/2211.09646, 2022. 2
- [11] Xi Chen, Xiao Wang, Soravit Changpinyo, AJ Piergiovanni, Piotr Padlewski, Daniel Salz, Sebastian Goodman, Adam Grycner, Basil Mustafa, Lucas Beyer, et al. Pali: A jointly-scaled multilingual language-image model. *arXiv preprint arXiv:2209.06794*, 2022. 2
- [12] Yen-Chun Chen, Linjie Li, Licheng Yu, Ahmed El Kholy, Faisal Ahmed, Zhe Gan, Yu Cheng, and Jingjing Liu. Uniter: Universal image-text representation learning. In *ECCV*, 2020. 3, 6
- [13] Yuxuan Ding, Lingqiao Liu, Chunna Tian, Jingyuan Yang, and Haoxuan Ding. Don’t stop learning: Towards continual learning for the clip model. *arXiv:2207.09248*, 2022. 2
- [14] Anuj Diwan, Layne Berry, Eunsol Choi, David F. Harwath, and Kyle Mahowald. Why is winoground hard? investigating failures in visuolinguistic compositionality. In *Conference on Empirical Methods in Natural Language Processing*, 2022. 2, 7, 8, 3, 5
- [15] Alexey Dosovitskiy, Lucas Beyer, Alexander Kolesnikov, Dirk Weissenborn, Xiaohua Zhai, Thomas Unterthiner, Mostafa Dehghani, Matthias Minderer, Georg Heigold, Sylvain Gelly, Jakob Uszkoreit, and Neil Houlsby. An image is worth 16x16 words: Transformers for image recognition at scale. *ICLR*, 2021. 4
- [16] Sivan Dohav, Assaf Arbelle, Sivan Harary, Rameswar Panda, Roei Herzig, Eli Schwartz, Donghyun Kim, Raja Giryes, Rogerio Feris, Shimon Ullman, et al. Teaching structured vision&language concepts to vision&language models. *arXiv preprint arXiv:2211.11733*, 2022. 2, 3, 4, 6
- [17] Chen Gao, Jiarui Xu, Yuliang Zou, and Jia-Bin Huang. Drg: Dual relation graph for human-object interaction detection. *ArXiv*, abs/2008.11714, 2020. 3
- [18] Yuting Gao, Jinfeng Liu, Zihan Xu, Jun Zhang, Ke Li, and Chunhua Shen. Pyramidclip: Hierarchical feature alignment for vision-language model pretraining. *arXiv preprint arXiv:2204.14095*, 2022. 2, 3
- [19] Chunjiang Ge, Rui Huang, Mixue Xie, Zihang Lai, Shiji Song, Shuang Li, and Gao Huang. Domain adaptation via prompt learning. *arXiv preprint arXiv:2202.06687*, 2022. 3
- [20] Rohit Girdhar, Joao Carreira, Carl Doersch, and Andrew Zisserman. Video action transformer network. In *Proceedings of the IEEE Conference on Computer Vision and Pattern Recognition*, pages 244–253, 2019. 3

- [21] Rohit Girdhar, Deva Ramanan, Abhinav Kumar Gupta, Josef Sivic, and Bryan C. Russell. Actionvlad: Learning spatio-temporal aggregation for action classification. *2017 IEEE Conference on Computer Vision and Pattern Recognition (CVPR)*, pages 3165–3174, 2017. 3
- [22] Shashank Goel, Hritik Bansal, Sumit Bhatia, Ryan A Rossi, Vishwa Vinay, and Aditya Grover. Cyclip: Cyclic contrastive language-image pretraining. *arXiv preprint arXiv:2205.14459*, 2022. 2, 3
- [23] Patrick Helber, Benjamin Bischke, Andreas Dengel, and Damian Borth. Eurosat: A novel dataset and deep learning benchmark for land use and land cover classification. *IEEE Journal of Selected Topics in Applied Earth Observations and Remote Sensing*, 12(7):2217–2226, 2019. 7
- [24] Roei Herzig, Ofir Abramovich, Elad Ben-Avraham, Assaf Arbelle, Leonid Karlinsky, Ariel Shamir, Trevor Darrell, and Amir Globerson. Promptonomyvit: Multi-task prompt learning improves video transformers using synthetic scene data. 2022. 2, 3
- [25] Roei Herzig, Amir Bar, Huijuan Xu, Gal Chechik, Trevor Darrell, and Amir Globerson. Learning canonical representations for scene graph to image generation. In *European Conference on Computer Vision*, 2020. 2, 3
- [26] Roei Herzig, Elad Ben-Avraham, Karttikeya Mangalam, Amir Bar, Gal Chechik, Anna Rohrbach, Trevor Darrell, and Amir Globerson. Object-region video transformers. In *Conference on Computer Vision and Pattern Recognition (CVPR)*, 2022. 3
- [27] Roei Herzig, Elad Levi, Huijuan Xu, Hang Gao, Eli Brosh, Xiaolong Wang, Amir Globerson, and Trevor Darrell. Spatio-temporal action graph networks. In *Proceedings of the IEEE International Conference on Computer Vision Workshops*, pages 0–0, 2019. 3
- [28] Roei Herzig, Moshiko Raboh, Gal Chechik, Jonathan Berant, and Amir Globerson. Mapping images to scene graphs with permutation-invariant structured prediction. In *Advances in Neural Information Processing Systems (NIPS)*, 2018. 3
- [29] Neil Houlsby, Andrei Giurgiu, Stanislaw Jastrzebski, Bruna Morrone, Quentin De Laroussilhe, Andrea Gesmundo, Mona Attariyan, and Sylvain Gelly. Parameter-efficient transfer learning for NLP. In *Proceedings of the 36th International Conference on Machine Learning*, pages 2790–2799, 2019. 3
- [30] Edward J Hu, Yelong Shen, Phillip Wallis, Zeyuan Allen-Zhu, Yuanzhi Li, Shean Wang, Lu Wang, and Weizhu Chen. Lora: Low-rank adaptation of large language models. *arXiv preprint arXiv:2106.09685*, 2021. 3, 5
- [31] Gabriel Ilharco, Mitchell Wortsman, Ross Wightman, Cade Gordon, Nicholas Carlini, Rohan Taori, Achal Dave, Vaishaal Shankar, Hongseok Namkoong, John Miller, Hananeh Hajishirzi, Ali Farhadi, and Ludwig Schmidt. Openclip, July 2021. 7, 4
- [32] Achiya Jerbi, Roei Herzig, Jonathan Berant, Gal Chechik, and Amir Globerson. Learning object detection from captions via textual scene attributes. *ArXiv*, abs/2009.14558, 2020. 3
- [33] Jingwei Ji, Ranjay Krishna, Li Fei-Fei, and Juan Carlos Niebles. Action genome: Actions as composition of spatio-temporal scene graphs. *arXiv preprint arXiv:1912.06992*, 2019. 3
- [34] Chao Jia, Yinfei Yang, Ye Xia, Yi-Ting Chen, Zarana Parekh, Hieu Pham, Quoc Le, Yun-Hsuan Sung, Zhen Li, and Tom Duerig. Scaling up visual and vision-language representation learning with noisy text supervision. In *International Conference on Machine Learning*, pages 4904–4916. PMLR, 2021. 2, 3, 4
- [35] Menglin Jia, Luming Tang, Bor-Chun Chen, Claire Cardie, Serge Belongie, Bharath Hariharan, and Ser-Nam Lim. Visual prompt tuning. In *European Conference on Computer Vision (ECCV)*, 2022. 2, 3
- [36] Justin Johnson, Agrim Gupta, and Li Fei-Fei. Image generation from scene graphs. In *Proceedings of the IEEE conference on computer vision and pattern recognition*, pages 1219–1228, 2018. 3
- [37] Justin Johnson, Ranjay Krishna, Michael Stark, Li-Jia Li, David Shamma, Michael Bernstein, and Li Fei-Fei. Image retrieval using scene graphs. In *Proceedings of the IEEE conference on computer vision and pattern recognition*, pages 3668–3678, 2015. 3
- [38] Chen Ju, Tengda Han, Kunhao Zheng, Ya Zhang, and Weidi Xie. Prompting visual-language models for efficient video understanding. In *European Conference on Computer Vision (ECCV)*, 2022. 3
- [39] Keizo Kato, Yin Li, and Abhinav Gupta. Compositional learning for human object interaction. In *ECCV*, 2018. 3
- [40] Wonjae Kim, Bokyung Son, and Ildoo Kim. Vilt: Vision-and-language transformer without convolution or region supervision. In *Proceedings of the 38th International Conference on Machine Learning*, pages 5583–5594, 2021. 6
- [41] Diederik P Kingma and Jimmy Ba. Adam: A method for stochastic optimization. *arXiv preprint arXiv:1412.6980*, 2014. 4
- [42] Ranjay Krishna, Ines Chami, Michael S. Bernstein, and Li Fei-Fei. Referring relationships. *ECCV*, 2018. 3
- [43] Ranjay Krishna, Yuke Zhu, Oliver Groth, Justin Johnson, Kenji Hata, Joshua Kravitz, Stephanie Chen, Yannis Kalantidis, Li-Jia Li, David A Shamma, et al. Visual genome: Connecting language and vision using crowdsourced dense image annotations. *International Journal of Computer Vision*, 123(1):32–73, 2017. 1, 2, 7, 4, 6
- [44] Alex Krizhevsky, Geoffrey Hinton, et al. Learning multiple layers of features from tiny images. 2009. 7
- [45] Brian Lester, Rami Al-Rfou, and Noah Constant. The power of scale for parameter-efficient prompt tuning. In *Proceedings of the 2021 Conference on Empirical Methods in Natural Language Processing*, pages 3045–3059, Online and Punta Cana, Dominican Republic, Nov. 2021. Association for Computational Linguistics. 3
- [46] Chunyuan Li, Haotian Liu, Liunian Harold Li, Pengchuan Zhang, Jyoti Aneja, Jianwei Yang, Ping Jin, Yong Jae Lee, Houdong Hu, Zicheng Liu, and Jianfeng Gao. Elevater: A benchmark and toolkit for evaluating language-augmented visual models. *Neural Information Processing Systems*, 2022. 7

- [47] Junnan Li, Dongxu Li, Caiming Xiong, and Steven Hoi. Blip: Bootstrapping language-image pre-training for unified vision-language understanding and generation. *arXiv preprint arXiv:2201.12086*, 2022. [2](#), [3](#), [4](#), [5](#), [6](#), [7](#), [8](#), [1](#)
- [48] Liunian Harold Li, Mark Yatskar, Da Yin, Cho-Jui Hsieh, and Kai-Wei Chang. Visualbert: A simple and performant baseline for vision and language. *ArXiv*, abs/1908.03557, 2019. [3](#)
- [49] Rongjie Li, Songyang Zhang, and Xuming He. Sgtr: End-to-end scene graph generation with transformer. *2022 IEEE/CVF Conference on Computer Vision and Pattern Recognition (CVPR)*, pages 19464–19474, 2021. [2](#)
- [50] Xiujun Li, Xi Yin, Chunyuan Li, Xiaowei Hu, Pengchuan Zhang, Lei Zhang, Lijuan Wang, Houdong Hu, Li Dong, Furu Wei, Yejin Choi, and Jianfeng Gao. Oscar: Object-semantic aligned pre-training for vision-language tasks. *ECCV 2020*, 2020. [2](#), [3](#)
- [51] Yong-Lu Li, Liang Xu, Xinpeng Liu, Xijie Huang, Yue Xu, Mingyang Chen, Ze Ma, Shiyi Wang, Hao-Shu Fang, and Cewu Lu. Hake: Human activity knowledge engine. *arXiv preprint arXiv:1904.06539*, 2019. [7](#), [4](#)
- [52] Zhaojiang Lin, Andrea Madotto, and Pascale Fung. Exploring versatile generative language model via parameter-efficient transfer learning. In *Findings*, 2020. [3](#)
- [53] Fangyu Liu, Guy Edward Toh Emerson, and Nigel Collier. Visual spatial reasoning. *ArXiv*, abs/2205.00363, 2022. [2](#), [3](#), [6](#)
- [54] Ilya Loshchilov and Frank Hutter. Decoupled weight decay regularization. In *International Conference on Learning Representations*, 2017. [4](#)
- [55] Chih-Yao Ma, Asim Kadav, Iain Melvin, Zsolt Kira, Ghasan Al-Regib, and Hans Peter Graf. Attend and interact: Higher-order object interactions for video understanding. *2018 IEEE/CVF Conference on Computer Vision and Pattern Recognition*, pages 6790–6800, 2018. [3](#)
- [56] Zixian Ma, Jerry Hong, Mustafa Omer Gul, Mona Gandhi, Irena Gao, and Ranjay Krishna. Crepe: Can vision-language foundation models reason compositionally? *ArXiv*, abs/2212.07796, 2022. [2](#)
- [57] Rabeeh Karimi Mahabadi, Sebastian Ruder, Mostafa Dehghani, and James Henderson. Parameter-efficient multi-task fine-tuning for transformers via shared hypernetworks. In *Annual Meeting of the Association for Computational Linguistics*, 2021. [3](#)
- [58] E. Mavroudi, Benjamín Béjar Haro, and René Vidal. Representation learning on visual-symbolic graphs for video understanding. In *ECCV*, 2020. [3](#)
- [59] Tushar Nagarajan, Yanghao Li, Christoph Feichtenhofer, and Kristen Grauman. Ego-topo: Environment affordances from egocentric video. *2020 IEEE/CVF Conference on Computer Vision and Pattern Recognition (CVPR)*, pages 160–169, 2020. [3](#)
- [60] Khoi Pham, Kushal Kaffle, Zhe Lin, Zhihong Ding, Scott Cohen, Quan Tran, and Abhinav Shrivastava. Learning to predict visual attributes in the wild. In *Proceedings of the IEEE/CVF Conference on Computer Vision and Pattern Recognition*, pages 13018–13028, 2021. [7](#), [4](#)
- [61] Sarah Pratt, Mark Yatskar, Luca Weihs, Ali Farhadi, and Aniruddha Kembhavi. Grounded situation recognition. In *European Conference on Computer Vision*, pages 314–332. Springer, 2020. [7](#), [4](#)
- [62] Moshiko Raboh, Roei Herzig, Gal Chechik, Jonathan Berant, and Amir Globerson. Differentiable scene graphs. In *WACV*, 2020. [3](#)
- [63] Alec Radford, Jong Wook Kim, Chris Hallacy, Aditya Ramesh, Gabriel Goh, Sandhini Agarwal, Girish Sastry, Amanda Askell, Pamela Mishkin, Jack Clark, et al. Learning transferable visual models from natural language supervision. In *International Conference on Machine Learning*, pages 8748–8763. PMLR, 2021. [2](#), [3](#), [4](#), [5](#), [6](#), [7](#), [8](#)
- [64] Sylvestre-Alvise Rebuffi, Hakan Bilen, and Andrea Vedaldi. Learning multiple visual domains with residual adapters. In *NIPS*, 2017. [3](#)
- [65] Hamid Rezatofighi, Nathan Tsoi, JunYoung Gwak, Amir Sadeghian, Ian Reid, and Silvio Savarese. Generalized intersection over union. In *The IEEE Conference on Computer Vision and Pattern Recognition (CVPR)*, June 2019. [7](#), [1](#)
- [66] Olga Russakovsky, Jia Deng, Hao Su, Jonathan Krause, Sanjeev Satheesh, Sean Ma, Zhiheng Huang, Andrej Karpathy, Aditya Khosla, Michael Bernstein, et al. Imagenet large scale visual recognition challenge. *International journal of computer vision*, 115(3):211–252, 2015. [7](#)
- [67] Victor Sanh, Albert Webson, Colin Raffel, Stephen Bach, Lintang Sutawika, Zaid Alyafeai, Antoine Chaffin, Arnaud Stiegler, Arun Raja, Manan Dey, M Saiful Bari, Canwen Xu, Urmish Thakker, Shanya Sharma Sharma, Eliza Szczechla, Taewoon Kim, Gunjan Chhablani, Nihal Nayak, Debajyoti Datta, Jonathan Chang, Mike Tian-Jian Jiang, Han Wang, Matteo Manica, Sheng Shen, Zheng Xin Yong, Harshit Pandey, Rachel Bawden, Thomas Wang, Trishala Neeraj, Jos Rozen, Abheesht Sharma, Andrea Santilli, Thibault Fevry, Jason Alan Fries, Ryan Teehan, Teven Le Scao, Stella Biderman, Leo Gao, Thomas Wolf, and Alexander M Rush. Multitask prompted training enables zero-shot task generalization. In *International Conference on Learning Representations*, 2022. [3](#)
- [68] Christoph Schuhmann, Richard Vencu, Romain Beaumont, Robert Kaczmarczyk, Clayton Mullis, Aarush Katta, Theo Coombes, Jenia Jitsev, and Aran Komatsuzaki. Laion-400m: Open dataset of clip-filtered 400 million image-text pairs. *arXiv preprint arXiv:2111.02114*, 2021. [1](#), [2](#), [7](#)
- [69] Sheng Shen, Chunyuan Li, Xiaowei Hu, Yujia Xie, Jianwei Yang, Pengchuan Zhang, Anna Rohrbach, Zhe Gan, Lijuan Wang, Lu Yuan, et al. K-lite: Learning transferable visual models with external knowledge. In *NeurIPS*, 2022. [2](#)
- [70] James Smith, Paola Cascante-Bonilla, Assaf Arbelle, Donghyun Kim, Rameswar Panda, David Cox, Diyi Yang, Zsolt Kira, Rogério Schmidt Feris, and Leonid Karlinsky. Construct-vl: Data-free continual structured vl concepts learning. *ArXiv*, abs/2211.09790, 2022. [3](#)
- [71] Chen Sun, Abhinav Shrivastava, Carl Vondrick, Kevin Murphy, Rahul Sukthankar, and Cordelia Schmid. Actor-centric relation network. In *Proceedings of the European Conference on Computer Vision (ECCV)*, pages 318–334, 2018. [3](#)

- [72] Yi-Lin Sung, Jaemin Cho, and Mohit Bansal. VI-adapter: Parameter-efficient transfer learning for vision-and-language tasks. *2022 IEEE/CVF Conference on Computer Vision and Pattern Recognition (CVPR)*, pages 5217–5227, 2021. 3
- [73] Yi-Lin Sung, Varun Nair, and Colin Raffel. Training neural networks with fixed sparse masks. In *Neural Information Processing Systems*, 2021. 3
- [74] Hao Tan and Mohit Bansal. Lxmert: Learning cross-modality encoder representations from transformers. pages 5099–5110. Association for Computational Linguistics, 2019. 3, 6
- [75] Bugra Tekin, Federica Bogo, and Marc Pollefeys. H+o: Unified egocentric recognition of 3d hand-object poses and interactions. *2019 IEEE/CVF Conference on Computer Vision and Pattern Recognition (CVPR)*, pages 4506–4515, 2019. 3
- [76] Tristan Thrush, Ryan Jiang, Max Bartolo, Amanpreet Singh, Adina Williams, Douwe Kiela, and Candace Ross. Winoground: Probing vision and language models for visiolinguistic compositionality. In *Proceedings of the IEEE/CVF Conference on Computer Vision and Pattern Recognition*, pages 5238–5248, 2022. 2, 3, 7, 8, 5
- [77] Ashish Vaswani, Noam Shazeer, Niki Parmar, Jakob Uszkoreit, Llion Jones, Aidan N Gomez, Łukasz Kaiser, and Illia Polosukhin. Attention is all you need. In I. Guyon, U. V. Luxburg, S. Bengio, H. Wallach, R. Fergus, S. Vishwanathan, and R. Garnett, editors, *Advances in Neural Information Processing Systems*, volume 30. Curran Associates, Inc., 2017. 4
- [78] Xiaolong Wang and Abhinav Gupta. Videos as space-time region graphs. In *ECCV*, 2018. 3
- [79] Chao-Yuan Wu and Philipp Krähenbühl. Towards Long-Form Video Understanding. In *CVPR*, 2021. 3
- [80] Bingjie Xu, Yongkang Wong, Junnan Li, Qi Zhao, and M. Kankanhalli. Learning to detect human-object interactions with knowledge. *2019 IEEE/CVF Conference on Computer Vision and Pattern Recognition (CVPR)*, pages 2019–2028, 2019. 3
- [81] Danfei Xu, Yuke Zhu, Christopher B. Choy, and Li Fei-Fei. Scene Graph Generation by Iterative Message Passing. In *CVPR*, pages 3097–3106, 2017. 2, 3, 5
- [82] Keyulu Xu, Jingling Li, Mozhi Zhang, Simon S. Du, Kenichi Kawarabayashi, and Stefanie Jegelka. What can neural networks reason about? In *International Conference on Learning Representations*, 2020. 3
- [83] Jingkang Yang, Yi Zhe Ang, Zujin Guo, Kaiyang Zhou, Wayne Zhang, and Ziwei Liu. Panoptic scene graph generation. In *European Conference on Computer Vision*, 2022. 2
- [84] Mert Yuksekgonul, Federico Bianchi, Pratyusha Kalluri, Dan Jurafsky, and James Zou. When and why vision-language models behave like bags-of-words, and what to do about it? In *International Conference on Learning Representations*, 2023. 2, 3, 4, 5
- [85] Mert Yuksekgonul, Federico Bianchi, Pratyusha Kalluri, Dan Jurafsky, and James Y. Zou. When and why vision-language models behave like bags-of-words, and what to do about it? *ArXiv*, abs/2210.01936, 2022. 2
- [86] Vinicius Zambaldi, David Raposo, Adam Santoro, Victor Bapst, Yujia Li, Igor Babuschkin, Karl Tuyls, David Reichert, Timothy Lillicrap, Edward Lockhart, et al. Relational deep reinforcement learning. *arXiv preprint arXiv:1806.01830*, 2018. 3
- [87] Rowan Zellers, Mark Yatskar, Sam Thomson, and Yejin Choi. Neural motifs: Scene graph parsing with global context. In *Conference on Computer Vision and Pattern Recognition*, 2018. 2
- [88] Yubo Zhang, Pavel Tokmakov, Martial Hebert, and Cordelia Schmid. A structured model for action detection. In *2019 IEEE/CVF Conference on Computer Vision and Pattern Recognition (CVPR)*, pages 9967–9976, 2019. 3
- [89] Tiancheng Zhao, Tianqi Zhang, Mingwei Zhu, Haozhan Shen, Kyusong Lee, Xiaopeng Lu, and Jianwei Yin. VI-checklist: Evaluating pre-trained vision-language models with objects, attributes and relations. *arXiv preprint arXiv:2207.00221*, 2022. 2, 3, 7, 4
- [90] Kaiyang Zhou, Jingkang Yang, Chen Change Loy, and Ziwei Liu. Conditional prompt learning for vision-language models. *2022 IEEE/CVF Conference on Computer Vision and Pattern Recognition (CVPR)*, pages 16795–16804, 2022. 2, 3
- [91] Kaiyang Zhou, Jingkang Yang, Chen Change Loy, and Ziwei Liu. Conditional prompt learning for vision-language models. In *IEEE/CVF Conference on Computer Vision and Pattern Recognition (CVPR)*, 2022. 3
- [92] Kaiyang Zhou, Jingkang Yang, Chen Change Loy, and Ziwei Liu. Learning to prompt for vision-language models. *Int. J. Comput. Vis.*, 130:2337–2348, 2022. 2, 3

## Supplementary Material for “SGVL”

In this supplementary file, we provide additional information about our experimental results, qualitative examples, implementation details, and datasets. Specifically, Section A provides more additional method details, Section B provides more experiment results, Section C provides qualitative visualizations to illustrate our approach, and Section D provides additional implementation details.

### A. Additional Method Details

We begin by presenting additional model details regarding our graph preprocessing procedure (section A.1). Next, we explain in detail our method for creating graph-based negatives (section A.2), which is illustrated in Figure 4. We conclude by giving more details on our scene graph loss (section A.3) and some modifications made to our loss calculation when training BLIP [47] (section A.4).

#### A.1. Graph Preprocessing

We next describe how we process the image-SG pairs to create our training dataset. Our guiding principle is to create image-SG training pairs where the graphs are dense enough but not too large, in order to allow structured and short descriptions. To this end, given an image  $I$  and a corresponding graph  $G(V, E)$ , we extract the sub-graphs by taking a random walk on the graph. The random walk is initialized by randomly picking a relationship from the graph (edge  $e \in E$  and nodes  $v_1, v_2 \in V$  such that  $e = (v_1, v_2)$ ) and ends when a node that has no outgoing edges is reached, resulting in a sub-graph  $G_1 = (V_1, E_1)$ . Next, the image is cropped to the union of the bounding boxes of all objects ( $v \in V_1$ ) in the extracted sub-graph, resulting image  $I_1$ . We finish the process by adding new nodes and relationships to  $G_1$  from the residual graph  $G_r = (V/V_1, E/E_1)$  that are visible in  $I_1$ . We use  $G_1$  and  $I_1$  as a training sample only if the derived  $G_1$  contains at most 10 objects (i.e.  $|E_1| \leq 10$ ). This process creates SGs composed of connected components that are all DAGs with a single Hamiltonian path, which facilitates caption generation.

#### A.2. Graph-Based Negatives

In order to generate negative image captions, we propose a set of predefined rules that when applied to an image-scene graph pair, result in a negative scene graph that incorrectly describes the image. Our scene graph to caption scheme transforms negative scene graphs into negative captions that are semantically inconsistent with the images they accompany. For each training sample we randomly apply one of the following negative rules focused on object attributes and relationships in the graph: (i) *asymmetric relations swapping* - we call a relationship  $R$  asymmetric, if for two objects  $a, b$ ,  $aRb \implies \neg bRa$ . We manually annotated

a relation as asymmetric out of the 300 most common VG relations. We use these to generate a negative scene graph by searching for an edge  $e = (v_1, v_2) \in E$  representing an asymmetric relationship, and modify the graph by replacing  $e$  with an edge  $e_n = (v_2, v_1)$ . For example, in the case of a graph describing the phrase “dog chasing cat”, such a negative will result in the phrase “cat chasing dog”. (ii) *relation falsification* - we replace relations in the graph with false relations. For example, we turn “cup on table” to “cup under table”. For negatives focused on object attributes, we first scan the dataset and split the attributes into the following categories: *color, material, size, state*. Next, we use this split to perform two types of negatives: (i) *attributes falsification* - we replace attributes for objects in the graph with false attribute from the same category. For example, turning “blue ball” to “red ball”. (ii) *attributes swapping* - we search the graph for two objects that are annotated with attributes from the same category. Given that such a pair has been found we switch between the attributes, resulting for example, “silver spoon and golden knife” from “golden spoon and silver knife”.

#### A.3. Scene Graph Loss

We need to match the predictions of the SG tokens with the ground-truth SG, in order to determine which SG tokens correspond to which ground-truth objects and relationships. We follow the matching approach as in DETR [9], except that in our case, objects and relationships are matched separately. We describe the object matching below. Given a permutation  $\sigma$  over the object queries, we define the matching-cost between the permutation and the GT by:

$$s(\sigma) = \sum_{i=1}^{\tilde{n}} \left[ \mathbb{1}_{\{o_i \neq \emptyset\}} \hat{q}_{\sigma(i)}^o(o_i) + \mathbb{1}_{\{o_i \neq \emptyset\}} \left( \lambda_{giou} \mathcal{L}_{giou}(b_i^o, \hat{b}_{\sigma(i)}) + \lambda_{l1} \|b_i^o - \hat{b}_{\sigma(i)}\|_1 \right) \right]$$

Namely, we check the compatibility between the GT and permuted objects both in terms of object category (i.e., the probability assigned by the query to the GT object  $o_i$ ) and in terms of bounding boxes (i.e., how well the predicted box matches the GT one). Here  $\mathcal{L}_{giou}$  is from [65], and  $\lambda_{l1}$  and  $\lambda_{giou}$  are hyperparameters.

The optimal matching  $\hat{\sigma}$  is found by optimizing this score:  $\hat{\sigma} = \arg \min_{\sigma \in \Sigma} s(\sigma)$ .

Finally, we use the optimal matching  $\hat{\sigma}$  from above to calculate the following Objects loss:

$$\mathcal{L}_{Objects} = \sum_{i=1}^{\tilde{n}} \left[ -\log \hat{q}_{\hat{\sigma}(i)}^o(o_i) + \mathbb{1}_{\{o_i \neq \emptyset\}} \left( \lambda_{giou} \mathcal{L}_{giou}(b_i^o, \hat{b}_{\hat{\sigma}(i)}) + \lambda_{l1} \|b_i^o - \hat{b}_{\hat{\sigma}(i)}\|_1 \right) \right]$$

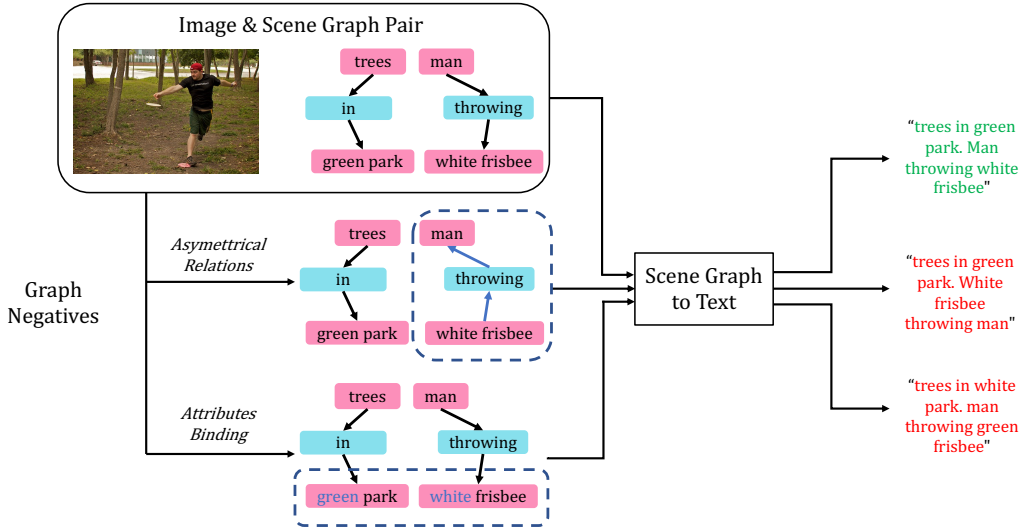


Figure 4: **Qualitative visualization** of the Graph-based Negatives and SG to Text modules. We show the generation process of positive captions (green) and negative captions using the graph (red).

The relation loss  $\mathcal{L}_{Rel}$  is calculated in a similar manner, and the total scene graph loss is the sum of  $\mathcal{L}_{Obj}$  and  $\mathcal{L}_{Rel}$ :

$$\mathcal{L}_{SG} := \mathcal{L}_{Obj} + \mathcal{L}_{Rel} \quad (12)$$

Finally, we optimize our final loss as the sum of the scene graph loss and the image-text loss:

$$\mathcal{L}_{Total} := \mathcal{L}_{IT} + \lambda_{SG} \mathcal{L}_{SG} \quad (13)$$

#### A.4. BLIP Image-Text Loss Details

Besides image and text unimodal encoders trained using a contrastive loss, BLIP [47] also includes an image-grounded text encoder that uses additional image-text cross-attention layers. The encoder is equipped with a binary classification head (a linear layer) and is trained to predict whether an image-text pair is positive (matching) or negative (unmatching). In the training procedure described by the authors, the encoder uses a hard negative mining strategy to calculate an additional loss for all image-text pairs in the batch. When training our BLIP-SGVL model, we apply this loss as well. Additionally, we use this encoder to add another term to our graph-based negative loss ( $\mathcal{L}_{GN}$ ). Let  $E_{IT}^P(I, T)$  denote the positive score given by the encoder to the image-text pair  $(I, T)$ , then the following term is added to  $\mathcal{L}_{GN}$ :

$$\sum_{I_G, T^P, T^n} -\log \left( \frac{e^{E_{IT}^P(I_G, T^P)}}{e^{E_{IT}^P(I_G, T^P)} + e^{E_{IT}^P(I_G, T^n)}} \right) \quad (14)$$

## B. Additional Experiment Results

We begin by presenting additional results (Section B.1). Next, we present additional ablations (Section B.2) we performed in order to test the contribution of the different SGVL components.

### B.1. Additional Results

We start by presenting additional results from two recent datasets: the ARO and the VSR datasets, which demonstrate that our approach works on a variety of datasets. We then show additional results on all splits in Winoground.

**The ARO and VSR datasets.** To further evaluate our proposed SGVL approach, we experiment on two recent benchmarks: the ARO [85] and the VSR [53] datasets in Table 5.

For the ARO dataset (more details are in Section D.3), we test our models on the *COCO Order* and *Flickr30K* tasks, that test the ability of VL models to identify the correct order of words in a caption. We compare our CLIP-SGVL and BLIP-SGVL models to the CLIP and BLIP baselines, as well as to the NegCLIP model [85], a variant of CLIP that was trained on the COCO dataset with hard negatives that were generated from the captions without using graph structure. It can be seen that our models significantly improve CLIP and BLIP baselines by +41.2 and +42.1 on COCO, and +31.5 and +39.7 on Flickr30K, respectively. Last, our CLIP-SGVL model also improves NegCLIP by +1.2 on COCO, demonstrating the effectiveness of our graph-based negative approach over some hard-negative mining as used in NegCLIP.

For the VSR dataset (more details are in Section D.4),

Model	ARO-PRC		VSR							
	COCO	Flickr30K	Adjacency	Directional	Orientation	Projective	Proximity	Topological	Unallocated	Average
Random Chance	20	20	50	50	50	50	50	50	50	50
CLIP [63]	46.0	59.5	-	-	-	-	-	-	-	-
NegCLIP [84]	86.0	91.0	-	-	-	-	-	-	-	-
BLIP [47]	24.9	27.9	55.4	48.9	53.7	58.2	56.5	55.6	63.4	56.5
CLIP-SGVL (ours)	87.2 (+41.2)	91.0 (+31.5)	-	-	-	-	-	-	-	-
BLIP-SGVL (ours)	67.0 (+42.1)	67.6 (+39.7)	58.2 (+2.8)	53.8 (+4.9)	57.0 (+3.3)	63.3 (+5.1)	58.4 (+1.9)	64.8 (+8.8)	70.0 (+6.6)	62.3 (+5.8)

Table 5: **Results on ARO and VSR.** We report accuracy on the ARO dataset [84] and VSR [53] datasets.

Model	Ambiguously Correct			Unusual Image			Unusual Text			Non Compositional			Visually Difficult			Complex Reasoning			No Tag		
	T	I	G	T	I	G	T	I	G	T	I	G	T	I	G	T	I	G	T	I	G
CLIP [63]	30.4	15.2	13.0	25.0	8.9	5.4	30.0	16.0	10.0	76.7	36.7	33.3	15.8	0.0	0.0	24.4	7.7	3.8	30.4	11.1	8.2
BLIP [47]	39.1	17.4	15.2	37.5	16.1	14.3	30.0	14.0	8.0	50.0	33.3	30.0	29.0	10.5	10.5	24.4	7.7	2.6	44.8	23.8	19.2
CLIP-SGVL (ours)	37.0	13.0	8.7	28.6	10.7	7.1	32.0	10.0	8.0	70.0	40.0	30.0	18.4	5.3	5.3	24.4	16.7	12.8	33.2	14.0	8.7
BLIP-SGVL (ours)	41.3	28.3	24.0	35.7	30.4	21.4	32.0	24.0	14.0	53.3	53.3	40.0	23.7	21.1	15.8	28.2	10.3	6.4	44.2	37.8	26.2

Table 6: **Results on Winoground** on all the splits. We report T, I, and G for Text retrieval, Image retrieval, and Group retrieval.

that checks the ability of VL models to correctly identify spatial relations in images, we compare our BLIP-SGVL model to the BLIP baseline. Our performance improves across all categories, including an average improvement of +5.8. We note that we could not evaluate CLIP since the task requires assigning a true or false label to an image-text pair. CLIP, however, does not allow this to be done in a straightforward manner.

**Winoground results.** We provide a complete analysis in Table 6 for all different splits, as reported in [14]. As can be seen, our SGVL approach is consistent across all splits.

## B.2. Additional Ablations

Next, we provide additional ablations that further illustrates the benefits of our SGVL.

**Training with negatives from non-graph data.** In order to demonstrate the importance of structured information in textual descriptions, we examine the performance of the model when only LAION captions are used. More specifically, we trained on generated negatives that were not derived from scene graph data but were generated in a similar manner to our graph-based negatives. Since we do not have the graphs in this setup, we apply the following augmentations: (i) swapping asymmetric relations - We swap the nouns that are relevant to the relation by using a standard parser. (ii) relation falsification - The relation is replaced with one from a closed set of relations we manually annotated in order to obtain the wrong semantic meaning. (iii) attributes swapping - We swap attributes from a closed set of attribute categories that we manually annotated (e.g., color, etc.). The Text/Image/Group scores compared

to the BLIP baseline are +4.0/-0.7/-0.8, while using BLIP with our graph-based augmentations (with SG tokens) obtains +1.5/+6.3/+3.2 compared to the BLIP baseline. It can be seen that the generated negatives from LAION improve only the Text score while applying our graph-based negatives improves all the metrics. This indicates that the main reason for the improvement is the structured information contained in the descriptions generated from the SGs.

**The importance of the scene graph data.** To examine the significance of the information provided by scene graphs, we suggest learning scene graphs without any useful information. Thus, we run an experiment in which the scene graphs are completely random. This ablation obtains on Winoground 37.8/18.7/14.0 compared to our BLIP-SGVL 39.0/30.5/21.5 for Text/Image/Group scores (the BLIP baseline obtains 39.0/19.2/15.0). This illustrates that the approach we employ is not merely a regularization, but also provides important information about the scene graphs that can be used by pretrained large VL models.

**The effect of image-SG data size.** In this experiment, we train our method using varying amounts of image-SG pairs of data (10%, 40%, 70%, and 100% of the dataset) in order to examine the effect of the data portion. Figure 5 shows the Winoground group score performance as a function of the image-SG pairs data portion. As can be seen, as more data is used, the results continue to improve, suggesting that adding image-SG data consistently leads to better results.

**The importance of simultaneous training.** In our SGVL approach, as described in the main paper, we train with the original image-text pairs from LAION as well as the image-SG pairs from Visual Genome simultaneously. To

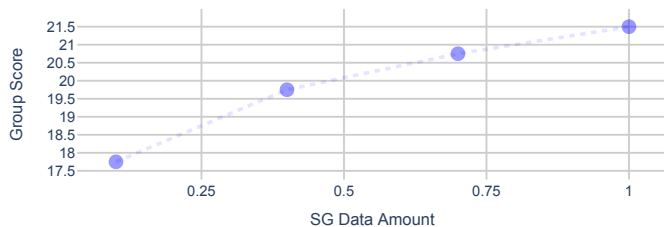


Figure 5: **Image-SG Pair Data Size.** We report the performance of our model on Winoground group score as a function of the amount of scene-graph data used during training (percentage of the available data).

verify the effectiveness of simultaneous training, we train only with VG data and obtain a degradation of -2.0/-1.2/-1.7 for Text/Image/Group scores compared to our BLIP-SGVL. In addition, we observe a degradation of 3% in zero-shot performance when compared to our BLIP-SGVL model. The results indicate that training on image-text pairs from LAION and image-SG pairs from Visual Genome simultaneously is crucial for performance and zero-shot.

**Token specialization.** Our SGVL approach learns a different specialization for each scene graph token in Figure 6. We visualize the box predicted by 10 different object tokens and 7 random relationship tokens for all images in the COCO val set. We observe that these tokens are specialized in different locations in the image, whereas the relationship tokens tend to be centered since their boxes are larger and spread over a greater area.

**Scene graph token representations.** To verify what the scene graph tokens learned, we can evaluate the ability of object and relationship tokens to be utilized explicitly for the auxiliary task as a simple scene graph predictor in images. This is accomplished by predicting the scene graphs on Visual Genome based on the learned SG tokens. We compared the learned SG tokens with a BLIP model extended with object and relationship heads. Our model achieved an mAP of 17.3, while the proposed baseline achieved an mAP of 14.4. These results indicate that the SG tokens learn meaningful and useful representations.

### C. Qualitative Visualizations

Figure 4 shows a visualization of the generation process of captions, including positive captions as well as negative captions, based on our Graph-based Negatives module. As shown in the figure, captions generated from scene graphs are much more focused on describing fine-grained details. Furthermore, we show in Figure 7 visualizations of “scene graph tokens” predictions for images from Visual Genome, which the model was not trained on. It can be seen that although the model has not been trained on these images, the predictions are reasonable. Finally, we show in Figure 8 and Figure 9 error analysis on Winoground

and VL-Checklist to evaluate the success and errors of our method and the baselines. This illustrates which examples our model succeeds on while the BLIP model fails.

## D. Additional Implementation Details

Our SGVL model can be used on top of the most common VL models (e.g., CLIP [63], BLIP [47], ALIGN [34]). For our experiments, we choose the CLIP [63] and BLIP [47] models as they are among the most popular and easy-to-use methods. These models are implemented based on the Open-CLIP library [31] and the BLIP code base (available at <https://github.com/salesforce/BLIP>), and we implement SGVL based on these repositories. As described above, our approach is trained using both the original image-text pairs from LAION and the image-SG pairs from the Visual Genome. In particular, we use for CLIP-SGVL 3M image-text pairs, while for BLIP-SGVL, we use 750K due to computational constraints.

In our experiments, we trained our CLIP-SGVL on 4 RTX 3090 GPUs for 32 epochs with a batch comprised of 256 image-text pairs and 8 image-SG pairs. We use AdamW optimizer [41, 54] with  $\beta_1 = 0.9$ ,  $\beta_2 = 0.98$ , and  $\epsilon = 1e - 6$ . We use  $lr = 1e - 4$  with cosine scheduler, and a weight decay of 0.2 for regularization. For BLIP-SGVL, we trained on 4 RTX 3090 GPUs for 16 epochs with a batch comprised of 32 image-text pairs and 8 image-SG pairs. We use AdamW optimizer [41] with  $\beta_1 = 0.9$ ,  $\beta_2 = 0.99$ , and  $\epsilon = 1e - 8$ . We use  $lr = 1e - 4$  with cosine scheduler, and a weight decay of 0.05 for regularization.

Last, we set the number of object and relationship tokens to 25 and 7, respectively. We also set the LoRA ranks for  $r_{SG} = 32$  and  $r_p = 16$ , and the  $\lambda$  parameters (see Equation 7 and Equation 13) for  $\lambda_{GN}$  to 1.0 and  $\lambda_{SG}$  to 0.1. Next, we elaborate on the additional implementation details for each dataset, including inference information.

### D.1. VL-Checklist

**Dataset.** VL-Checklist [89] is a new study that combines the following datasets: Visual Genome [43], SWiG [61], VAW [60], and HAKE [51] datasets. For each image, two captions are given, a positive and a negative. The positive caption is derived from the source dataset and is coherent with the visual structure of the image. The negative caption is constructed by modifying one word in the positive caption that corresponds to a structural aspect in the image. To correctly solve a sample the model needs to identify the caption faithfully describing the image. Specifically, VL-Checklist evaluates the following structured concepts: (1) Object: identifying objects invariantly to their spatial location and size, (2) Relation: spatial or action relation between two objects, and (3) Attribute: color, material, size, state, and action bounded to objects. In the following sections, we report results on a combined VL-Checklist dataset



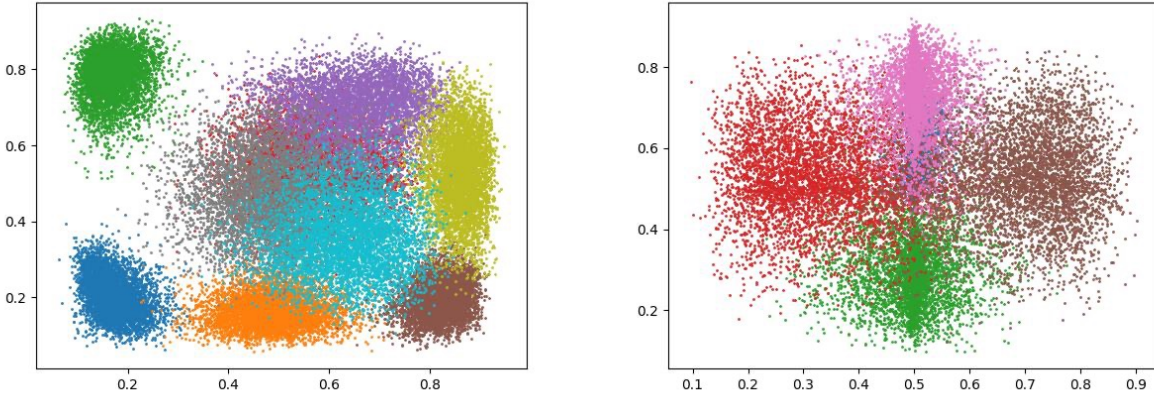


Figure 6: **Tokens Specialization.** We visualize the box predictions of 10 random object tokens (left) and 7 relationship tokens (right) on all images from the COCO validation set. Each box is represented as a point with the normalized coordinates of its center. Colors indicate the predictions made by different tokens.

excluding Visual Genome.

**Inference details.** A test sample consists of an image and two captions. For CLIP, we compute the cosine similarity between the image and the captions and report the positive caption as the one with the higher similarity. For BLIP, we use the ITM head, which predicts both a positive and negative score for each pair. We consider the caption with the higher positive score to be the correct one.

## D.2. Winoground

**Dataset.** Winoground [76] is a new challenging dataset that evaluates the ability of VL models to capture compositionality in vision & language. The dataset contains 400 samples, each composed of two image-text pairs  $(I_0, C_0), (I_1, C_1)$ . The pairs have overlapping lexical content but are differentiated by a swapping of an object, a relation, or both. To correctly solve the sample the model needs to correctly solve two text retrieval and two image retrieval tasks. A recent study [14] has shown that solving Winoground requires not just compositional understanding but also other abilities such as commonsense reasoning. The study proposed a new split to the dataset differentiating the samples by the source of their hardness. Specifically, the split of the samples into the following categories is as follows: *Non Compositional* - There are 30 samples in this category that do not require compositional reasoning. *Visually Difficult* - The model must be able to detect an item that is visually difficult to identify (small, blurry, in the background, etc.) in order to sort these samples correctly. This category includes 38 samples. *Ambiguously Correct* - This category includes 46 samples where at least one caption accurately describes both images or doesn't quite describe any of the images. *Unusual Text & Unusual Image* - There are

106 samples in these categories, all of which contain unrealistic or awkward texts or images that make it difficult to solve them with a VL model. *Complex Reasoning* - This category consists of 78 samples that require common sense reasoning or knowledge of the world around us. *No Tag* - These are vanilla Winoground examples that solely probe compositional understanding.

**Inference details.** For testing, the pairs are given, and a text score, an image score, and a group score for a sample is computed in the following way: The text score is 1 if and only if image  $I_0$  has a higher similarity to caption  $C_0$  than  $C_1$ , and image  $I_1$  has a higher similarity to caption  $C_1$  than  $C_0$ . Similarly the image score is 1 if and only if caption  $C_0$  has a higher similarity to image  $I_0$  than image  $I_1$  and  $C_1$  has a higher similarity to image  $I_1$  than image  $I_0$ . The group score is 1 if and only if both text and image scores are 1. Thus, the random chances for both the image and text score, is  $1/4$  while for group score it is  $1/6$ . Similarities between image-text pairs is computed as in section D.1.

## D.3. ARO

**Dataset.** ARO [84] (Attribution, Relation, and Order) is a new benchmark that tests compositionality in VL models. This dataset consists of four large-scale tasks designed to test the relational, attributive, and order understanding of the model. For evaluation, the authors propose four tasks that are sensitive to order and composition, namely Visual Genome Relation, Visual Genome Attribution, COCO& Flickr30k Order. Since our approach is trained on Visual Genome, we report only the COCO and Flickr30k order task (PRC). For the order task, image-text pairs from the mentioned datasets are used. The words in the text are re-ordered in order to create false captions for the image, ac-

ording to the following perturbations: *nouns and adjectives shuffle*, *everything but nouns and adjectives shuffle*, *trigrams shuffle* and *words within trigrams shuffle*.

**Inference details.** During inference, each sample consists of an image and five textual descriptions. The similarity of each text to the image is measured as in section D.1, and the text with the highest similarity to the image is reported as the real caption.

#### D.4. VSR

**Dataset.** VSR [53] VSR (Visual Spatial Reasoning) is a new benchmark for measuring the spatial understanding of vision-language models. The VSR dataset consists of natural image-text pairs in English, each example contains an image and a natural language description of the spatial relationship between two objects shown in the image. The VL model needs to classify images and captions as either true or false, indicating whether a caption accurately describes the spatial relationship. The dataset has more than 10K image-text samples, derived from 6,940 COCO images and covers 65 spatial relations. The dataset is split into a train, validation and test sets, however, since we evaluate in a zero-shot manner we test our model and baselines using all samples from the train, validation, and test splits. The spatial relations are divided into 7 meta-categories: *Adjacency*, *Directional*, *Orientation*, *Projective*, *Proximity*, *Topological*, *Unallocated*. We report results according to these categories, as well as the average over all spatial relations.

**Inference details.** We do not evaluate CLIP on this task since the task requires assigning a true or false label to an image-text pair. CLIP, however, does not allow this to be done in a straightforward manner, and Therefore only the BLIP model can be used. We use the ITM head to determine whether the sample is true or false, as done in [47].

#### D.5. Scene Graph Datasets

In our work, we use the LAION dataset as “standard” image-text pairs, along with image-SG data pair from Visual Genome [43] (VG). Visual Genome is annotated with 108,077 images accompanied by their corresponding scene graphs. On average, images have 35 entities, 21 relationships, and 26 attributes per image. Additionally, there are approximately 70K object categories and 40K relationship categories. In general, Visual Genome scene graphs can be viewed as dense knowledge representations for images, similar to the format used for knowledge bases in natural language processing.

#### D.6. Licenses and Privacy

The license, PII, and consent details of each dataset are in the respective papers. In addition, we wish to emphasize that the datasets we use do not contain any harmful or offensive content, as many other papers in the field also use

them. Thus, we do not anticipate a specific negative impact, but, as with any Machine Learning method, we recommend to exercise caution.



Figure 7: **Scene Graph Prediction.** We show the predictions of the “scene graph tokens” on images from Visual Genome that were not trained by our model.



Figure 8: **Error Analysis on Winoground.** We demonstrate on the left in green where our BLIP-SGVL model succeeds, while the baseline BLIP model fails. On the right, in red, we can observe examples in which our BLIP-SGVL model fails. As visible, are model improves in samples that require understanding relations between objects, binding attributes to objects, and counting objects.

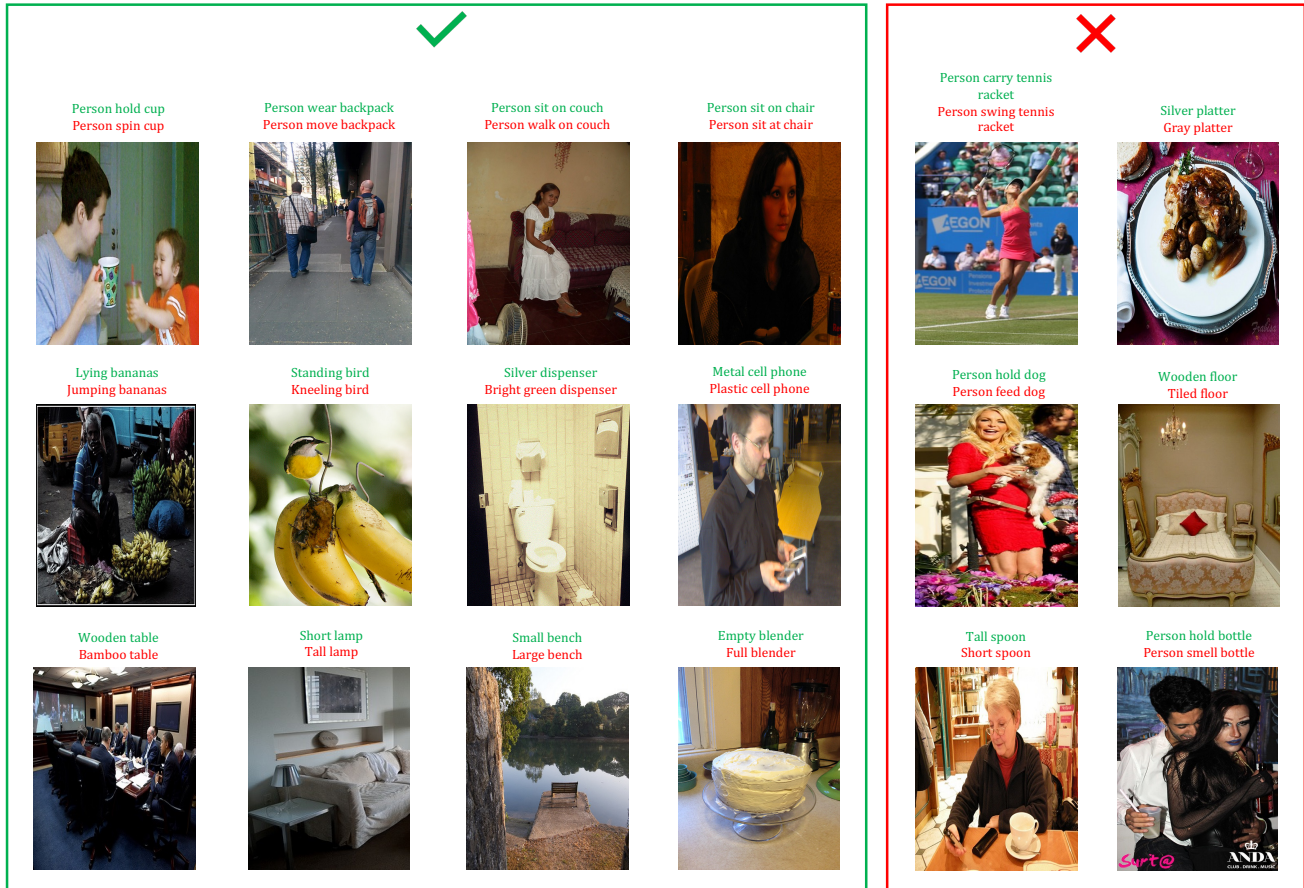


Figure 9: **Error Analysis on VL-Checklist.** We demonstrate on the left in green where our BLIP-SGVL model succeeds, while the baseline BLIP model fails. On the right, in red, we can observe examples in which our BLIP-SGVL model fails. As visible, some of the samples on which our model fails are ambiguous or visually difficult to solve.